DARTs and CORK in Cascadia Basin: High-resolution observations of the 2004 Sumatra tsunami in the northeast Pacific

Alexander Rabinovich,[1,2] Kelly Stroker,[3] Richard Thomson,[1] and Earl Davis[4]

Received 9 February 2011; revised 8 March 2011; accepted 11 March 2011; published 21 April 2011.

[1] We report unique deep-sea recordings of the Sumatra tsunami of December 2004 by high-resolution DART® (Deep-ocean Assessment and Reporting of Tsunami) and CORK (Circulation Obviation Retrofit Kit) bottom pressure sensors deployed at depths of ~1500–3500 m in Cascadia Basin in the northeast Pacific. The simultaneous records from these sites establish the first-ever regional-scale tsunami detection array for the open ocean, enabling us to resolve both seafloor and crustal tsunami signals and to determine fundamental properties of the waves following their 22,000 km journey from the source region. Waves reaching the basin had mean amplitudes of ~5 mm with energy spread over a broad frequency band from 0.4 to 7 cph. Peak tsunami energy was in the 0.8 to 2 cph (75 to 30 min) band. Leading waves from the event arrived 34–35 h after the earthquake, roughly 7 h later than expected, suggesting that the tsunami mainly propagated by the "most economic" (minimum energy loss) path along mid-ocean ridge wave-guides rather than taking the direct and fastest path across the ocean. Motions within the peak energy band comprise roughly 50% coherent progressive waves propagating from the south at longwave phase speeds of ~150 ms^{-1} and 50% random waves scattered from the coast and bottom irregularities. Tsunami amplitudes in the borehole were one-third those on the seafloor. The extensive "ringing" and anomalously slow (3.5-day) *e*-folding decay time of the tsunami wave energy indicates long duration energy flux radiating from the Indian Ocean via the Southern Pacific Ocean.
Citation: Rabinovich, A., K. Stroker, R. Thomson, and E. Davis (2011), DARTs and CORK in Cascadia Basin: High-resolution observations of the 2004 Sumatra tsunami in the northeast Pacific, *Geophys. Res. Lett.*, *38*, L08607, doi:10.1029/2011GL047026.

1. Introduction

[2] The catastrophic Sumatra tsunami of 26 December 2004 was recorded by coastal tide gauges throughout the World Ocean [cf. *Merrifield et al.*, 2005; *Woodworth et al.*, 2005; *Rabinovich et al.*, 2006; *Rabinovich and Thomson*, 2007; *Candella et al.*, 2008]. However, waves measured by these gauges were affected by local resonant effects, refraction, and nonlinearity [*Mofjeld*, 2009]. As a consequence, the records provide limited information on fundamental tsunami properties and source characteristics. In contrast, data from open-ocean bottom pressure recorders (BPRs) are highly valuable for determining the physical aspects of the source region and for contributing to real-time tsunami warning [*Bernard et al.*, 2001; *Titov*, 2009]. Here, we combine 15-sec, 0.1 mm depth resolution records from five BPRs in Cascadia Basin to determine the open-ocean properties of the 2004 tsunami.

[3] The DART® network provides open-ocean tsunami data in real time [*Bernard et al.*, 2001; *Mofjeld*, 2009]. At the time of the 2004 event, there were six U.S. DART® stations in the Pacific Ocean (Figure 1). Stations 46403 and 46405 were triggered by seismic waves, which arrived from the source region about 30 min after the earthquake. The stations subsequently transmitted five hours of data with 1-min sampling but then, the day before the tsunami arrival, returned to 15-min mode sampling [*Gower and González*, 2006]. The high-frequency (15-sec) data stored in the instrument packages were retrieved at the end of 2006 (see http://www.ndbc.noaa.gov/dart.shtml). However, due to technical factors, the 15-sec data were available only for station 46405 located at 3480 m depth near the axis of the Juan de Fuca Ridge (Figure 1) and for the New Millennium Observatory (NeMO) (http://www.pmel.noaa.gov/vents/nemo) located at depth of 1510 m in a submarine volcano caldera roughly 336.5 km northward of 46405.

[4] Deep-sea recordings of the 2004 tsunami were also available from CORK hydrologic observatories [*Davis et al.*, 2000; *Davis and Becker*, 2007] mounted within two Ocean Drilling Program (ODP) boreholes on the eastern Juan de Fuca Ridge flank. CORK stations 1026B (seafloor and borehole pressure recorders) with 15-sec and 1301A (seafloor) with 1-min samplings were located 1.5 km apart at a depth of 2658 m, about 271 km from NeMO. The four stations constitute an obtuse-angle sensor array (Figure 1) representing a high-resolution regional-scale tsunami detection system that enables us to delineate tsunami parameters undisturbed by coastal effects.

2. Tsunami Detection

[5] The extraction of tsunami signals from sea level records is generally hindered by low tsunami to background (signal-to-noise, S/N) ratios. Preliminary tsunami data analyses are therefore required to diminish the background noise level without distorting the tsunami signal. As indicated by Table 1, tides (red line in Figure 2a) account for ~99.9%

[1]Department of Fisheries and Oceans, Institute of Ocean Sciences, Sidney, British Columbia, Canada.
[2]P.P. Shirshov Institute of Oceanology, Russian Academy of Sciences, Moscow, Russia.
[3]National Geophysical Data Center, National Oceanic and Atmospheric Administration, Boulder, Colorado, USA.
[4]Pacific Geoscience Centre, Natural Resources Canada, Sidney, British Columbia, Canada.

0094-8276/11/2011GL047026

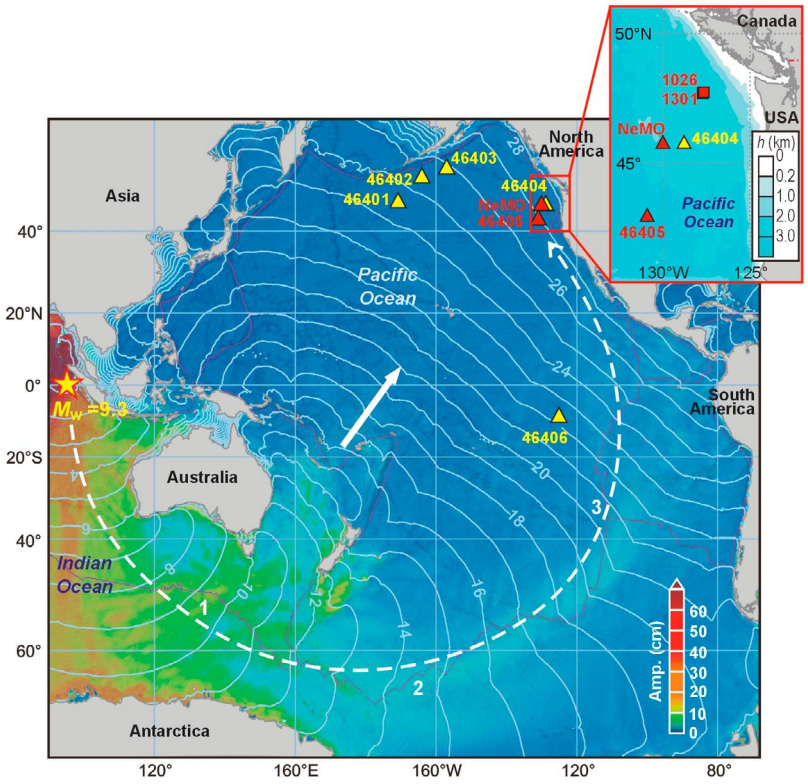

Figure 1. Locations of bottom pressure stations in the Pacific Ocean in December 2004 superimposed on the simulated 2004 tsunami wave heights [from *Titov et al.*, 2005]. Red triangles indicate the DART and NeMO stations that recorded 15-sec data, yellow triangles denote stations with 15-min data, and red squares the CORK stations 1026 and 1301 with 15-sec and 1-min data, respectively. The inset shows open-ocean stations in the northeast Pacific which recorded the 2004 tsunami. The isochrones (solid white lines) represent the tsunami travel time from the source area (the yellow star marks the 2004 Sumatra earthquake epicenter). The thick solid white arrow indicates the direction of the "fastest" tsunami propagation across the Pacific, while the dashed curved white arrow shows the computed tsunami energy flux propagating along the mid-ocean ridges; numbers denote the Southeast Indian Ridge (1), Pacific Antarctic Ridge (2), and East Pacific Rise (3).

of the long-wave energy in the study region. The residual series are mainly determined by low-frequency processes, likely of meteorological origin, with amplitudes of 1.5 to 4 cm. Following high-pass 4-hour filtering, the remaining energy variance diminished to 0.06–0.12 cm^2 (Table 1).

[6] The change in wave characteristics in the high-pass residual records (Figure 2a) marks the tsunami arrival time as 11:00–12:00 (UTC) on 27 December 2004. Additional 6-min low-pass filtering suppresses the high-frequency noise associated with infragravity waves [cf. *Webb et al.*, 1991], making the tsunami waves more evident (Figure 2b). These waves are accurately isolated in frequency-time ($f - t$) diagrams [cf. *Rabinovich et al.*, 2006] (Figure 2c), which show that the tsunami energy was concentrated in a broad frequency range with peak energy at 0.8–2.0 cph. The wave train structure of the records (with wave train lengths of 9–12 h) was apparently related to multiple tsunami reflections from continental borders and island chains [cf. *Kowalik*, 2008]. Although the root-mean-square (RMS) background noise in the tsunami band is statistically different at the four stations (due to differences in depth and instrument responses), the tsunami RMS (~3.1–3.4 mm) is similar for all seafloor instruments (Table 1). The mean tsunami amplitudes were ~5 mm, compared to 1 m for tides and 4 cm for low-frequency oscillations.

[7] Based on data from CORK site 1026B, the crustal response to the 2004 tsunami was attenuated by a factor three relative to the seafloor response over the entire tsunami

Table 1. Sea Level Variance at Different Stages of Analysis for Bottom Pressure Records

Station	Variances (cm^2) for the Period 24–30 December 2004				RMS (mm) of 24-hour Segments	
	Initial (With Tides)	De-tided (Residual)	High-Pass (4-hour) Filtered	Low-Pass (6-min) Filtered	Background	Tsunami
DART 46405	4336.4	6.92	0.060	0.043	1.37	3.11
NeMO	5720.9	5.70	0.097	0.053	1.79	3.38
CORK 1026B (sea floor)	7487.6	4.32	0.122	0.101	1.80	3.24
CORK 1026B (borehole)	769.3	0.93	0.111	0.010	0.73	1.07
CORK 1301A	7094.8	3.69	0.115	0.066	2.48	3.18

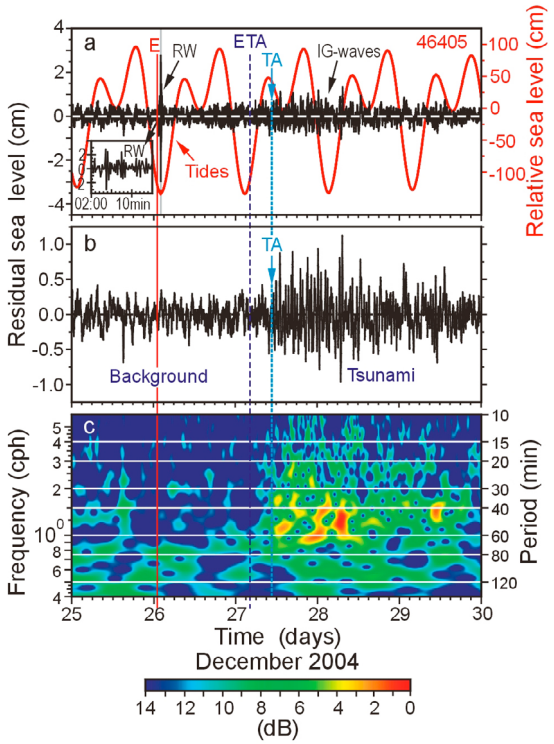

Figure 2. Recording of the 2004 Sumatra tsunami at DART station 46405 in the northeast Pacific. The solid red vertical line labelled "E" denotes the time of the earthquake; the dashed black vertical line indicates the Estimated time of Tsunami Arrival (ETA) and the dotted light-blue vertical line with an arrow indicates the actual tsunami arrival time (TA). (a) The original record is shown in red; the de-tided and high-pass filtered (4-hour KB-window) record is in black. The black arrow denotes the arrival of the seismic Rayleigh waves (RW) [cf. *Filloux*, 1982]; the inset provides a 15-min record of the RW waves; (b) the same record used in Figure 2a but after low-pass filtering with a 6-min KB window; and (c) frequency-time ($f-t$) plot of the tsunami record.

frequency band. Tides experience the same attenuation (Table 1), consistent with poroelastic loading [*Davis et al.*, 2000]. Borehole tsunami wave amplitudes were only about 1.5 mm but phases closely matched those at the seafloor at both 1026B and 1301A. This appears to be the first time that tsunami waves have been recorded within a borehole.

3. Analysis

[8] The first tsunami waves reached DART 46405 around 11:00 (UTC) on 27 December 2004, ~34 h after the earthquake. About 30 min later, these waves reached NeMO and then, 30 min later, sites 1026B and 1301A. The actual Tsunami Arrival times (TA) of 34–35 h are in agreement with those for coastal tide gauges on the West Coast [*Rabinovich et al.*, 2006], but 7–8 h longer than the Estimated time of Tsunami Arrival (ETA). Moreover, the roughly 30-min lags between the arrivals times at sites 46405, NeMO, and 1026B/1301A indicates general northward wave propagation, in agreement with the results of numerical modeling for this region (Figure 1), but contrary to the northeastward wave propagation for the ETA isochrones (thin white lines in Figure 1). The isochrones, calculated using Huygens principle, represent the quickest tsunami propagation route from the source area [*Murty*, 1977]. The observed 7–8 h time difference suggests that the identified tsunami waves traveled by the "most economic" (minimum energy loss) path rather than by the fastest route. (Waves which would have arrived by the fastest route appear to have been below detection levels.) The observed travel times agree with global tsunami propagation models [*Titov et al.*, 2005; *Kowalik*, 2008], which show that mid-ocean ridges served as wave-guides for the 2004 tsunami, efficiently transmitting the tsunami energy from the source area in the Indian Ocean to far-field regions in the Pacific and Atlantic oceans. In particular, the tsunami energy flux entering the Pacific Ocean from the southeastern Indian Ocean was directed counterclockwise around the Pacific Ocean, guided by the Southeast Indian Ridge, Pacific Antarctic Ridge, and East Pacific Rise (dashed white line in Figure 1).

[9] The tsunami (S_{tsu}) and background (S_{bg}) spectra for stations 46405 and NeMO are presented in Figures 3a and

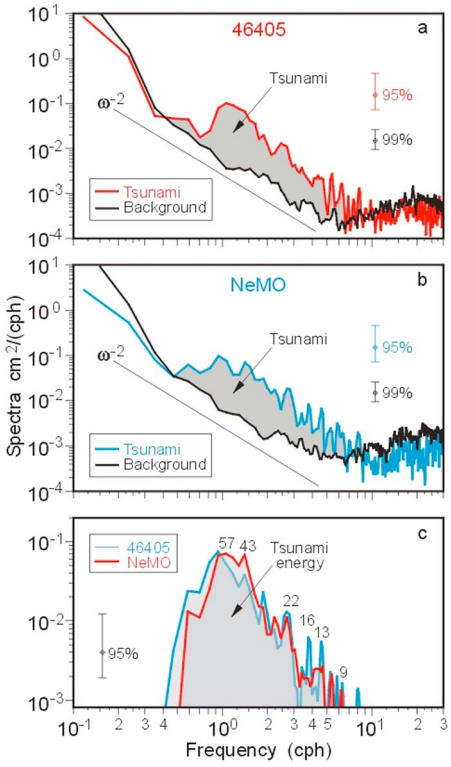

Figure 3. Spectral analyses of the background (pre-tsunami) and tsunami oscillations recorded at open-ocean stations (a) DART 46405 and (b) NeMO. (c) The "true" tsunami spectra at these stations estimated by subtraction of the background spectra from the observed tsunami spectra. The spectral "humps" in Figures 3a and 3b associated with the tsunami are shaded; a reference power law ω^{-2} is denoted. The numbers in Figure 3c indicate periods (in min) of the main tsunami peaks. Also shown are the 95% and 99% confidence levels for the tsunami and background spectra, respectively.

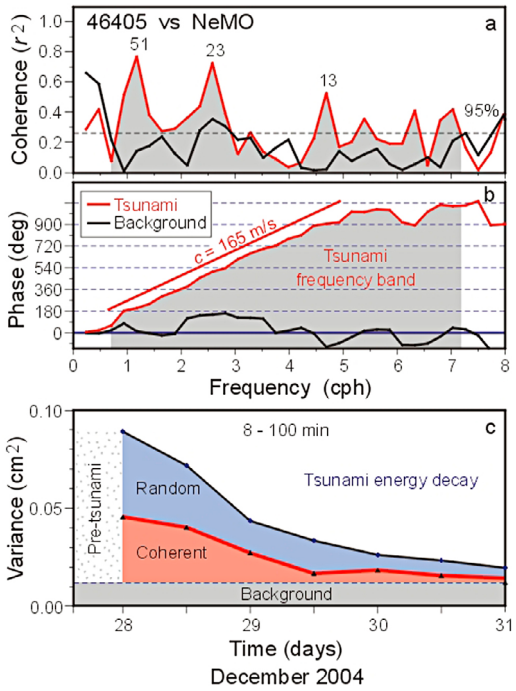

Figure 4. DART 46405 versus NeMO cross-spectral analyses for the background (black line) and tsunami oscillations (red line): (a) Coherence and (b) phase difference between the DART and NeMO time series. The straight line in Figure 4b denotes a non-dispersive phase speed of 165 ms^{-1} toward the north; numbers indicate periods (in min) of the main coherence peaks. The shaded area denotes the tsunami frequency band. (c) Time decay of the tsunami energy at station 46405. The "coherent" energy (red shading) is determined from cross-spectral analysis between the 46405 and NeMO records; the background energy level (flat grey region) is from pre-tsunami observations. The "random" tsunami energy (blue shading) is the difference between the total and coherent tsunami energy levels.

3b. Background spectra have been determined using four-day pre-tsunami data segments, while tsunami spectra have been estimated from one-day data immediately following the first wave arrival. The background spectra decrease monotonically with frequency as ω^{-2}, typical of longwave spectra for the open ocean [cf. *Kulikov et al.*, 1983]. The tsunami spectra match the background spectra at low and high frequencies but, at intermediate frequencies, have a prominent "bulge" associated with the tsunami. The "true" tsunami spectra, $\hat{S}_{tsu} = S_{tsu} - S_{bg}$ (Figure 3c), shows that the tsunami energy spanned the band 0.4 to 7 cph (periods 2.5 h to 8 min) both at the seafloor and in the underlying crust (where the wave energy was attenuated by a factor of 10). More than 90% of this energy was in frequencies 0.9 to 2 cph (periods 70 to 30 min), with peaks at periods of around 60 and 40 min. The true tsunami spectra, $\hat{S}_{tsu}$, were marginally affected by topographic variations in Cascadia Basin but unaffected by coastal and shelf effects. The dominant long periods were likely associated with the extensive (~1300 km) initial source area [*Stein and Okal*, 2005].

[10] Cross-spectral analyses between stations 46405, NeMO, and 1026B/1301A were used to examine the properties of propagating tsunami waves and the background noise. For the noise, the coherence (r^2) between oscillations at 46405 and NeMO is not statistically significant except at the lowest frequencies ($\omega < 0.6$ cph); in contrast, the tsunami records are coherent throughout most of the tsunami frequency band with peak $r^2 \sim 0.8$ (Figure 4a). The phase difference for tsunami waves in the 0.7–5 cph band changes almost linearly (Figure 4b) indicating non-dispersive tsunami waves propagating with long-wave phase speed $c = \sqrt{gH} \approx 165$ ms^{-1}. This speed corresponds to a depth $H = 2775$ m, which lies between the depth of 3430 m at station 46405 and 1510 m at NeMO. The non-dispersive character of the waves contrasts with the dispersive waves identified by *González and Kulikov* [1993] for the 1988 Alaskan Bight tsunami. We attribute this difference to the fact that the 2004 earthquake source was much larger, and the respective tsunami frequencies much lower, than for the 1988 event.

[11] Signal coherence between stations NeMO and 1026B/1301A was small for the background noise but significant for tsunami waves at frequencies 0.85–3.3 cph (periods 18 to 70 min). For the coherent frequency band, the phase changed linearly, consistent with a phase speed $c \approx 148$ ms^{-1}, corresponding to an "effective" depth $H = 2233$ m, which is bracketed by the station depth of 1510 m at NeMO and 2658 m at 1026B/1301A.

[12] According to our cross-spectral analyses, the energy flux propagated northward, in agreement with the observed tsunami arrival times and numerical modeling results (Figure 1). Computation of the cross-spectral characteristics for the second and the third days following arrival of the first tsunami wave shows that, while the coherence slowly decreased with time, the phases remained nearly constant, indicating a prolonged flux.

4. Discussion

[13] Integration of the true tsunami spectra (Figure 3c) and their "coherent" parts enabled us to examine tsunami energy decay within Cascadia Basin (Figure 4c). Perhaps the most pronounced feature to emerge from the records was the protracted (>3.5 days) tsunami ringing. Lengthy tsunami ringing reported earlier [cf. *Miller et al.*, 1962] was assumed to be related to wave trapping over the shelf. However, these effects cannot explain prolonged tsunami ringing in the deep ocean. The estimated *e*-folding "decay time", t_0, of the tsunami energy is 50.1 ± 2.7 h for DART 46405, 54.1 ± 2.4 h for NeMO, 56.1 ± 9.3 h for 1026B (seafloor), and 60.9 ± 12.2 h for 1301A. The larger uncertainties for the CORK stations are associated with higher noise levels.

[14] These t_0 values are approximately 2.5 times longer than $t_0 \approx 22$ h estimated by *Van Dorn* [1984] for the Pacific Ocean based on the "closed-room" acoustic analogy concept [*Munk*, 1963]. One possible reason for this difference is that the closed-room concept is an over-simplification for this particular event. In reality, the Pacific Ocean has a wide "entrance" connecting it to the Indian Ocean. Such abnormally long tsunami ringing and slow attenuation is only possible for long-duration external energy "pumping" through continued arrival of tsunami wave trains from the Indian Ocean, as well as from reflections and multiple paths within

the South Pacific and Southern Ocean (Figure 2c). Our analysis, together with recent numerical modeling by *Kowalik* [2008], validates this conclusion, indicating the presence of a prolonged northward directed energy flux (Figure 4c).

[15] The 2004 Indian Ocean tsunami was recorded with unprecedented clarity by an array of DART and ODP/CORK stations. Although the tsunami energy was only about 0.002% of the regional tidal energy, data analysis methodology made it possible to isolate and examine the tsunami waves. It is remarkable that, despite the 22,000 km travel distance and small heights (<2 cm), the 2004 tsunami was so clearly detectable. The deep-sea bottom pressure measurements provided by DART and CORK helps our understanding of tsunami physics and propagation characteristics. Early research on open-ocean tsunami waves was based on "solitary wave" theory. This was discounted by the first deep-sea measurements of local tsunamis [*Filloux*, 1982; *González et al.*, 1991] which demonstrated that open ocean tsunamis actually consist of a "train of long waves". Based on our analyses, it is clear that tsunamis (at least, major tsunamis) actually consist of a series of wave-trains associated with long-duration energy flux from the source region. Local and regional topographic features promote the formation of this flux, while mid-ocean ridges conserve and efficiently transmit the tsunami energy throughout the World Ocean.

[16] **Acknowledgments.** We thank Eddie Bernard, NOAA/PMEL (Seattle, WA) for initiating the global open-ocean tsunami monitoring program. We also thank Marie Eble for providing the NeMO data, Vasily Titov for making available his numerical modeling results, Isaac Fine for insightful discussions, Maxim Krassovski and Patricia Kimber for helping with the figures, and Frank González and one anonymous reviewer for their very useful comments.

[17] The Editor thanks Frank González and an anonymous reviewer for their assistance in evaluating this paper.

References

Bernard, E. N., F. I. González, C. Meinig, and H. B. Milburn (2001), Early detection and real-time reporting of deep-ocean tsunamis, in *Proceedings of the 2001 International Tsunami Symposium*, pp. 97–108, NOAA, Seattle, Wash.

Candella, R. N., A. B. Rabinovich, and R. E. Thomson (2008), The 2004 Sumatra tsunami as recorded on the Atlantic coast of South America, *Adv. Geosci.*, *14*(1), 117–128, doi:10.5194/adgeo-14-117-2008.

Davis, E. E., and K. Becker (2007), On the fidelity of "CORK" borehole hydrologic pressure records, *Sci. Drill.*, *5*, 54–59.

Davis, E. E., K. Wang, K. Becker, and R. Thomson (2000), Formation-scale hydraulic and mechanical properties of oceanic crust inferred from pore-pressure response to periodic seafloor loading, *J. Geophys. Res.*, *105*, 13,423–13,435, doi:10.1029/2000JB900084.

Filloux, J. H. (1982), Tsunami recorded on the open ocean floor, *Geophys. Res. Lett.*, *9*, 25–28, doi:10.1029/GL009i001p00025.

González, F. I., and E. A. Kulikov (1993), Tsunami dispersion observed in the deep ocean, in *Tsunamis in the World*, edited by S. Tinti, pp. 7–16, Kluwer, Dordrecht, Netherlands.

González, F. I., C. L. Mader, M. C. Eble, and E. N. Bernard (1991), The 1987–88 Alaskan Bight tsunamis: Deep ocean data and model comparisons, *Nat. Hazards*, *4*(2–3), 119–139, doi:10.1007/BF00162783.

Gower, J., and F. González (2006), U.S. Warning System detected the Sumatra tsunami, *Eos Trans. AGU*, *87*(10), doi:10.1029/2006EO100001.

Kowalik, Z. (2008), Energy flux as a tool in locating secondary sources, *Sci. Tsunami Hazards*, *27*, 1–29.

Kulikov, E. A., A. B. Rabinovich, A. I. Spirin, S. L. Poole, and S. L. Soloviev (1983), Measurements of tsunamis in the open ocean, *Mar. Geod.*, *6*, 311–329, doi:10.1080/15210608309379465.

Merrifield, M. A., et al. (2005), Tide gage observations of the Indian Ocean tsunami, December 26, 2004, *Geophys. Res. Lett.*, *32*, L09603, doi:10.1029/2005GL022610.

Miller, G. R., W. H. Munk, and F. E. Snodgrass (1962), Long-period waves over California's continental borderland. II. Tsunamis, *J. Mar. Res.*, *20*(1), 31–41.

Mofjeld, H. O. (2009), Tsunami measurements, in *The Sea*, vol. 15, *Tsunamis*, edited by A. Robinson and E. Bernard, pp. 201–235, Harvard Univ. Press, Cambridge, Mass.

Munk, W. H. (1963), Some comments regarding diffusion and absorption of tsunamis, *Proceedings of the Tsunami Meeting Associated With the Tenth Pacific Science Congress*, *Int. Union Geod. Geophys. Monogr.*, *24*, 53–72.

Murty, T. S. (1977), Seismic sea waves: Tsunamis, *Bull. 198*, 337 pp., Fish. Res. Board Can., Ottawa.

Rabinovich, A. B., and R. E. Thomson (2007), The 26 December 2004 Sumatra tsunami: Analysis of tide gauge data from the world ocean Part 1. Indian Ocean and South Africa, *Pure Appl. Geophys.*, *164*(2–3), 261–308, doi:10.1007/s00024-006-0164-5.

Rabinovich, A. B., R. E. Thomson, and F. E. Stephenson (2006), The Sumatra tsunami of 26 December 2004 as observed in the North Pacific and North Atlantic oceans, *Surv. Geophys.*, *27*, 647–677, doi:10.1007/s10712-006-9000-9.

Stein, S., and E. A. Okal (2005), Speed and size of the Sumatra earthquake, *Nature*, *434*, 581–582, doi:10.1038/434581a.

Titov, V. V. (2009), Tsunami forecasting, in *The Sea*, vol. 15, *Tsunamis*, edited by A. Robinson and E. Bernard, pp. 371–400, Harvard Univ. Press, Cambridge, Mass.

Titov, V. V., A. B. Rabinovich, H. Mofjeld, R. E. Thomson, and F. I. González (2005), The global reach of the 26 December 2004 Sumatra tsunami, *Science*, *309*, 2045–2048, doi:10.1126/science.1114576.

Van Dorn, W. G. (1984), Some tsunami characteristics deducible from tide records, *J. Phys. Oceanogr.*, *14*, 353–363, doi:10.1175/1520-0485(1984)014<0353:STCDFT>2.0.CO;2.

Webb, S. C., X. Zhang, and W. Crawford (1991), Infragravity waves in the deep ocean, *J. Geophys. Res.*, *96*, 2723–2736, doi:10.1029/90JC02212.

Woodworth, P. L., et al. (2005), Evidence for the Indonesian tsunami in British tidal records, *Weather*, *60*(9), 263–267, doi:10.1256/wea.59.05.

E. Davis, Pacific Geoscience Centre, Natural Resources Canada, PO Box 6000, Sidney, BC V8L 4B2, Canada.

A. Rabinovich and R. Thomson, Department of Fisheries and Oceans, Institute of Ocean Sciences, 9860 West Saanich Rd., Sidney, BC V8L 4B2, Canada. (alexander.rabinovich@dfo-mpo.gc.ca)

K. Stroker, National Geophysical Data Center, National Oceanic and Atmospheric Administration, 325 Broadway, Boulder, CO 80305-3328, USA.